J. COMBIN. MATH. COMBIN. COMPUT. 125 (2025) 5249--5275

Journal of Combinatorial Mathematics and Combinatorial Computing
www.combinatorialpress.com/jcmcc

Research on the construction of a computational model for assessing students' psychological state in ideological and political education of college students supported by multidimensional data

Beilei Qiao[1], Li Chang[1,✉]

[1] *Henan Agricultural University, Zhengzhou, Henan, 450046, China*

ABSTRACT

The accelerated pace of life and social competition become more and more intense, and the problem of psychological pressure faced by people in their study, work and life becomes more and more serious and common, this paper proposes a multi-channel physiological feature fusion method of psychological state assessment for the identification of students' psychological state in the ideological and political education of college students. The collected multidimensional physiological signal data, such as pulse and picoelectricity, are feature extracted, and the wavelet transform is used to reduce the noise of the physiological signals and realize the waveform filtering, and then the DS evidence theory is combined with the SVM, and the extracted physiological parameters of pulse and picoelectricity are used to realize the effective assessment of psychological stress. Experiments show that the method proposed in this paper of using wavelet decomposition coefficients instead of the original physiological signals as model input can improve the accuracy of psychological stress detection, and the MAPE value of psychological state assessment using the SVM-DS algorithm is 12.28%, which can realize the assessment of students' psychological state in ideological and political education of college students.

Keywords: physiological signal, feature extraction, wavelet transform, DS evidence theory, SVM, psychological state assessment

1. Introduction

In the concept of psychology, anxiety is a kind of normal emotional reaction of human beings, when people are in the middle of a difficult situation or have a bad premonition, anxiety will occur. Anxiety can help people better cope with the reality of difficulties, but if excessive anxiety, it will affect people's

✉ Corresponding author.
E-mail address: qbl921@126.com (L. Chang).
Received 12 January 2024; Revised 25 March 2024; Accepted 25 December 2024; Published Online 16 April 2025.
DOI: 10.61091/jcmcc127b-291

judgment of the outside world, if long-term anxiety, it will seriously disrupt people's normal life and work [1-3]. Mental health education plays an important role in promoting the development of students' mental health, which can prompt students to form a healthy mentality and sound personality [4]. Civic education can effectively improve the effect of mental health education, and both civic education and mental health education can promote the healthy development of college students, of which civic education is mainly to guide the students' thinking, prompting students to form correct values [5-6]. Mental health education is mainly to guide the students' psychological level, to ensure the students' mental health [7]. Therefore, the combination of ideological education and mental health education can not only promote the formation of correct values and enhance the innovation ability of college students, but also guide the healthy development of students [8-10]. In the current diversified environment, college students are more likely to be influenced by adverse information, and form incorrect outlooks or have psychological problems in a subtle way. Therefore, in the current situation, colleges and universities need to carry out mental health education on the basis of ideological education, so as to promote the physical and mental health development of college students [11-13].

This paper proposes a method of assessing students' psychological state in ideological and political education of college students based on physiological signals. Firstly, after selecting pulse and electrocardiogram as the analyzing signals, we analyze the generation, waveform and respective characteristics of various physiological signals and give the theoretical basis of physiological signal analysis and processing. Then, the method of collecting and pre-processing the physiological signals of students is researched, and the experimental scheme is designed to realize the collection of pulse and electrocardiogram signals, and then the statistical method is used to extract the characteristics of physiological signals, and the wavelet transform method is used to reduce the noise of the collected physiological signals. Subsequently, based on the physiological parameter characteristics of the three physiological signals of pulse and electrocardiogram, the decision layer fusion algorithm based on the combination of DS evidence theory and SVM is used to realize the effective assessment of psychological stress, and experiments are designed on this basis to test its performance. Finally, the psychological stress induction experiment is designed to establish a multimodal psychological stress detection dataset containing 115 times for the assessment of students' psychological state.

2. Student physiological signal processing and feature extraction with multidimensional data

2.1. Basis of physiological signal analysis

2.1.1. Theoretical Basis of Pulse Signal. Pulse (PPG) is the palpable beat of the arteries on the surface of the body. The circulatory system of the human body consists of the heart, blood vessels, and blood. Blood flows into the aorta through the contraction of the left ventricle of the heart, and then flows through the arteries throughout the body, and the arteries are dilated due to the pressure on the arteries, and the dilatation of arteries in the shallower parts of the body surface manifests itself in the form of the pulse. Pulse is a relatively stable quasi-periodic signal. Under normal circumstances, the pulse rate is basically the same as the heart rate, but it is susceptible to fluctuations within a certain range due to factors such as age, emotion, and behavior. A complete pulse waveform generally has three peaks B, D, F and two valleys C, E. According to these six points, the waveform is divided into five parts: main wave, pre-tidal trough, tidal wave, descending mid-isthmus and descending mid-wave, which represent different physiological significance, as shown in Table 1.

Table 1. Pulse signal characteristics point meaning

Characteristic point	Meaning

Ascending branch	A rise curve from the baseline to the top of the main crest of the pulse waveform is the rapid injection of the ventricle.
Drop branch	A descending curve in the pulse waveform from the host to the baseline is the beginning of the next phase of the ventricular injection.
Primary wave	The main body of the pulse graph, the peak of the general vertex is the peak of the pulse, reflecting the maximum pressure and volume of the artery.
Tidal wave	It is also called the prestroke wave, which is located in the descending branch, and after the main wave, it is generally lower than the host and is higher than the weight beat wave, which reflects the left ventricle stop the blood, the expansion of the artery, and the reverse reflection.
descending	It is also called the descending middle wave, which is the cutting trace of the main wave drop and the heavy bogorise, which indicates the time of the aorta, and the partition point for the contraction and relaxation of the heart.
Heavy wave	It is a rising wave in the descending branch, which is the main artery flap and the aorta elastic.

2.1.2. Theoretical Foundations of the Electrodermal Signal. Similar to the ECG signal, a typical pulse wave possesses the following characteristics:

1) Weak signal. Pulse signal is extremely weak, the amplitude range is only about 0-10mV, and because the signal is collected on the surface of the human body, so not only the collection equipment, electronic instruments, and other external conditions will affect its accuracy, and is susceptible to jitter, breathing, myoelectric signals from the body's own interference.

2) Low frequency. Pulse signals belong to the lower frequency infrasound, its frequency range of about 0-20Hz, of which 99% of the energy is concentrated in the 0-10Hz frequency range.

3) Variability. The pulse system is variable and unstable, and will be affected by the human body's physiological and psychological factors as well as the surrounding environment and show different pulse images, which can provide favorable characteristics for the study of human psychophysiology.

2.2. Physiological signal noise reduction processing

2.2.1. Continuous wavelet transform. Fourier transform, as a commonly used signal analysis method, can effectively link the signal time domain features and frequency domain features. In essence, it maps the time domain signal into a function in the frequency domain, thus realizing the transformation of time domain research to frequency domain research and revealing the spectral characteristics of the signal. The Fourier spectrum shows the statistical characteristics of the signal, which cannot effectively localize the signal and thus has certain limitations [14]. To compensate for this defect, wavelet analysis came into being. Wavelet analysis is a window size fixed its window function in the time domain plane with the change of the center frequency, in the high frequency at the time window becomes narrower, the low frequency at the frequency window edge narrower, to meet the analysis of mutant signals and non-smooth signals needs. Therefore, compared with other signal analysis methods, wavelets perform slightly better in eliminating motion artifacts and mitigating baseline drift.

Let the wavelet function be $\psi(t)$ and satisfy the condition:

$$C^{\psi} = \int_R \frac{|\psi^*(\omega)|}{|\omega|} d\omega < +\infty \tag{1}$$

Call $\psi(t)$ the parent wavelet function or wavelet basis, and obtain the family of functions after translation and scaling:

$$\psi_{az}(t) = \frac{1}{\sqrt{a}} \psi\left(\frac{t-\tau}{a}\right) a, \tau \in R, a \neq 0 \tag{2}$$

$\psi_{ax}(t)$ constitutes a set of orthogonal bases of the square productible space $L^2(R)$. The wavelet transform of a function $f(t) \in L^2(R)$ is defined as:

$$Wf(a,\tau) = < f, \psi_{a,\tau} > = \int_{-\infty}^{+\infty} \psi_{a,\tau}(t) f(t) dt \tag{3}$$

where, a is called the scale factor, the small scale wavelet transform contains the high frequency components of the signal, while the large scale wavelet transform contains the low frequency components of the signal; τ is the translation factor, which is the coefficient about the time, determining the time domain information of the wavelet transform, because the change of the two values presents a continuous state, so $\psi_{\alpha,t}(t)$ is called the continuous wavelet basis function.

$f(t)$ satisfies the square productability condition and $f(t) \in L^2(R)$, the continuous wavelet transform of the equation is:

$$WT_f(\alpha,\tau) = \langle f(t), \psi_{\alpha,\tau}(t) \rangle = \frac{1}{\sqrt{\alpha}} \int f(t) \psi^*(\frac{t-\tau}{\alpha}) dt \tag{4}$$

where $\psi(t)$ is the wavelet function, $\psi^*(t)$ is its complex conjugate. And $\alpha = 0,1,\tau$ are all continuous variables.

The convolutional expression of the continuous wavelet transform takes the form:

$$WT_f(\alpha,\tau) = \frac{1}{\sqrt{\alpha}} \int_{\mathrm{R}} f(t) \psi^*(\frac{t-\tau}{\alpha}) dt = |\alpha|^{1/2} f^* \bar{\psi}_{|\alpha|}(\tau) \tag{5}$$

where $\bar{\psi}_{|\alpha|}(\tau) = |\alpha|^{-1} f^* \psi^*_{|\alpha|}(-\tau/\alpha)$. In practical engineering, $\bar{\psi}_{|\alpha|}(\tau)$ can be interpreted as high-pass filtering.

2.2.2. Discrete wavelet transform. In the continuous wavelet transform, both scale factor a and translation factor τ vary continuously, thus greatly increasing the algorithmic computation. Not only that, the information processed by information processing tools such as MATLAB is discrete, thus a and τ need to be discretized. The specific process is:

Let $\alpha = \alpha_0^j, \tau = k\alpha_0^j b_0$ and assume $\alpha_0 > 1$.

Then the wavelet sequence formula is:

$$\psi_{j,k}(t) = \frac{1}{\sqrt{\alpha_0^j}} \psi(\frac{t - k\alpha_0^j b_0}{\alpha_0^j}) = \alpha_0^{\frac{-j}{2}} \psi(\alpha_0^{-j} t - kb_0), j,k \in Z \tag{6}$$

And the discrete wavelet transform coefficients can be expressed as:

$$C_{j,k}(f, \psi_{j,k}) = \sum_{n=-\infty}^{\infty} f(t) \psi^*_{j,k}(t) \tag{7}$$

where $\psi(t)$ is a wavelet basis function that satisfies certain conditions.

The inverse transform of the discrete wavelet transform is expressed as:

$$f(t) = \sum_{j=-\infty}^{\infty} \sum_{k=-\infty}^{\infty} C_{j,k} \psi_{j,k}(t) = \sum_{j=-\infty}^{\infty} f_j(t) \tag{8}$$

where $\psi_{j,k}(t) = 2^{-j/2} \psi(2^{-j} t - k)$, is the set of wavelet functions, j,k takes an integer, is the discretized scale $(\alpha = \alpha_0 2^j)$ and the time-shift parameter $(\tau = k\tau_0)$ and t is the continuous time variable. $f_j(t)$ denotes the component of the signal $f(t)$ on the j scale.

2.2.3. Wavelet denoising. The principle of wavelet denoising is mainly based on the low entropy and multi-scale characteristics of wavelets, the physiological signals are decomposed at multiple scales, and according to the differences in the frequency ranges of the target and interference signals, the target and interference signals are differentiated and processed, so as to effectively eliminate the noise. Physiological signals generated by the human body usually show low-frequency signals with stable waveforms, while noise signals usually show high-frequency signals with jumping waveforms. The threshold can be set reasonably for the difference of wavelet coefficients to achieve the purpose of filtering out noise signals.

And the threshold size is given by comparing the absolute value of the wavelet high frequency coefficients of the corresponding level, which can be divided into two kinds: soft threshold and hard threshold. Let w be the wavelet high-frequency coefficients, λ be the size of the threshold, and w_λ be the wavelet high-frequency coefficients after wavelet decomposition in the new wavelet high-frequency coefficients after threshold quantization. When $|w| \geq \lambda$, soft threshold denoising is the difference between the two as the new wavelet coefficients, while hard threshold denoising wavelet high frequency coefficients remain unchanged, and when $|w| < \lambda$, both are the wavelet high frequency coefficients are set to zero.

The formula for soft threshold quantization is as follows:

$$w_\lambda = \begin{cases} [sign(w)](|w| - \lambda) & |w| \geq \lambda \\ 0 & |w| < \lambda \end{cases} \tag{9}$$

The formula for hard threshold quantization is as follows:

$$w_\lambda = \begin{cases} w & |w| \geq \lambda \\ 0 & |w| < \lambda \end{cases} \tag{10}$$

2.3. Feature extraction of physiological signals

2.3.1. Event-related features:

1) Event-related features of the electrocardiogram signal. The PEEK signal can be decomposed into a gradient signal and a mutation signal, both of which can be used to extract event-related features, as shown in Fig. 1 (a) to (c) for the original signal, the mutation signal and the gradient signal, respectively. The gradient signal responds to the overall trend of signal change, and its 10-dimensional data features such as maximum, minimum, mean, median, standard deviation, variance, extreme distance, skewness, kurtosis, and plurality are used as the event-related features of the ECG signals, in which the skewness and kurtosis are calculated by the following formulas:

$$Skew = E\left[\left(\frac{x(t) - \mu}{\sigma}\right)^3\right] = \frac{E[(x(t) - \mu)^3]}{(E[(x(t) - \mu)^2])^{\frac{3}{2}}} \tag{11}$$

$$Kurt = E\left[\left(\frac{x(t) - \mu}{\sigma}\right)^4\right] = \frac{E[(x(t) - \mu)^4]}{(E[(x(t) - \mu)^2])^2} \tag{12}$$

where $x(t)$ represents the physiological signal, E is the mean of the signal, and μ represents the standard deviation.

The event-related features of the electrocardiogram (ECG) are also related to the skin conductance response (SCR), which embodies the rapidly changing part of the ECG signal, including the starting point, the peak and the half-life, and is able to sensitively reflect mood changes. By identifying the SCR in the EEG signal, extracting its rise time, half-life and peak, and calculating the maximum, minimum, mean, median, standard deviation, variance, polar distance, skewness, kurtosis, and multitude of the three, we obtained the 30-dimensional EEG's event-related features are also related to the skin conductance response (SCR), which embodies the fast-changing portion of the EEG signal, including the starting point, peak, and half-life, which can reflect mood changes sensitively. reflect mood changes. The 30-dimensional data features were obtained by identifying the SCR in the EEG signal, extracting its rise time, half-life and peak value, respectively, calculating the maximum, minimum, mean, median, standard deviation, variance, polar distance, skewness, kurtosis, and plurality of the three, and calculating the number of the SCRs and the integral area. In summary, a total of 42 event-related features of the picoelectric signal were obtained.

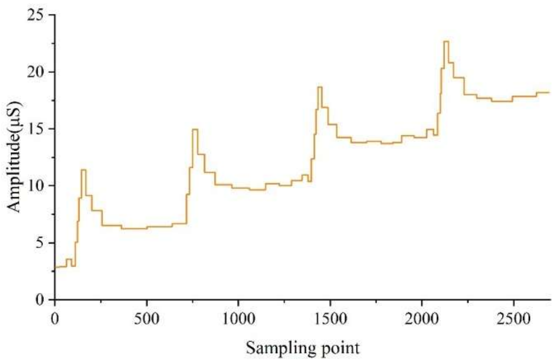

(a) Primary signal

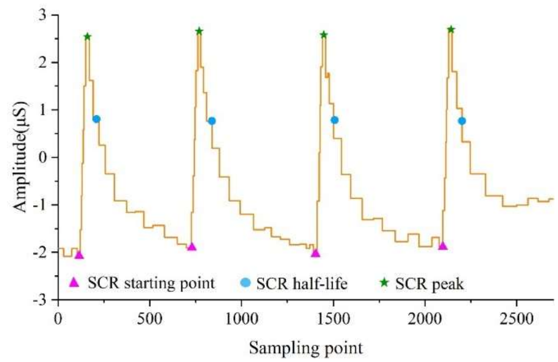

(b) Mutation signal

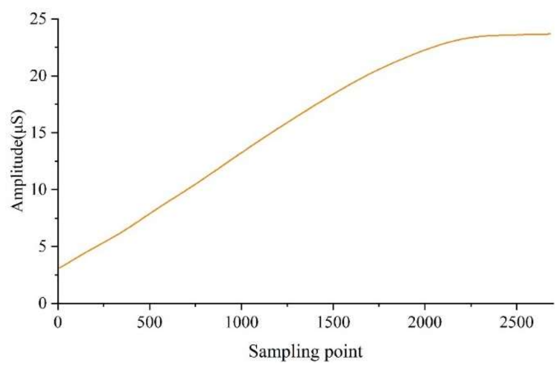

(c)Gradient signal

Fig. 1. SCR identification of leather

2) Event-related characteristics of pulse signals. Pulse signals are similar to ECG signals in that the waveform changes periodically with the heartbeat. Related studies have proved that the heart rate variability of pulse and ECG signals is related to emotional stress, and the event-related features of pulse signals are extracted using a feature extraction method similar to that of ECG signals.

The pulse signal waveform detection is shown in Figure 2. Compared with the ECG, the waveform structure of the pulse signal is relatively simple, and it is easier to obtain the position of the wave peak corresponding to each heartbeat to calculate the heart rate variability features. In addition to the heart rate variability features such as heart rate, standard deviation of the wave interval, square root of the successive differences of the wave interval, and standard deviation of the successive differences of the wave interval, the pulse signal is similarly analyzed nonlinearly, and the relevant features of the Poincare scatter plot and the difference scatter plot are computed, including short-term variability of the pulse, long-term variability, the cardiac vagal index, and the cardiac sympathetic index. From this, as with the ECG signal, the pulse signal was extracted totaling 44 dimensions of pulse signal event-related features.

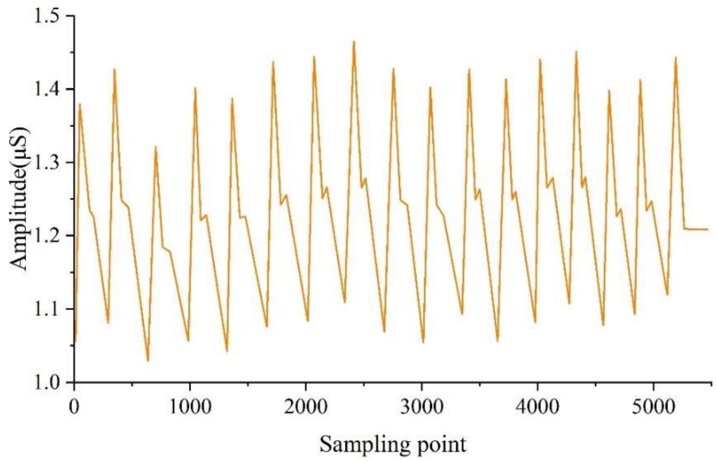

Fig. 2. Pulse signal wave peak detection

2.3.2. Statistical feature extraction methods. Physiological signal features also include statistical features, which respond to the overall trend of the waveform. Signal statistical features are extracted mainly by three methods: time domain analysis, frequency domain analysis and time-frequency domain analysis. Time domain analysis utilizes the waveform nature of the physiological signals to visualize the physical significance of the signals. In the time domain, 17-dimensional statistical features such as maximum, minimum, peak, peak-to-peak, mean, absolute mean, square root mean, variance, standard deviation, root mean square, crag, skewness, square root magnitude, waveform factor, peak factor, pulse factor, margin factor, etc., are calculated for each physiological signal, and the calculation formula is shown in Table 2.

Table 2. The formula for calculating the time domain characteristics of the physiological signal

Name	Formula
Peak	$X_{peak} = \max\{\lvert x_i \rvert\}$
Mean	$\bar{X} = \frac{1}{N}\sum_{t=1}^{N} x(t)$
Square amplitude	$X_{rms} = \left(\frac{1}{N}\sum_{t=1}^{N} x(t)^2\right)^2$
Waveform factor	$S_f = \frac{X_{rms}}{\lvert \bar{X} \rvert}$
Peak factor	$I_p = \frac{X_{peak}}{X_{rms}}$
Pulse factor	$C_f = \frac{X_{peak}}{\lvert \bar{X} \rvert}$
Margin factor	$C_e = \frac{X_{peak}}{X_{rms}}$

Physiological signals are more random and some information is not easily observed in the time domain and needs to be analyzed in the frequency domain. The physiological signals are projected onto the frequency domain by Fourier transform, and their power spectrum information is analyzed to extract the average frequency, the center of gravity frequency, the root mean square of the frequency and the standard deviation of the frequency features, and the calculation formula is shown below, where $P(f)$ is the power spectrum of the signal.

Center of gravity frequency:

$$FC = \frac{\int_0^{+\infty} f P(f) df}{\int_0^{+\infty} P(f) df} \tag{13}$$

Root mean square of frequency:

$$RMSF = \sqrt{\frac{\int_0^{+\infty} f^2 P(f) df}{\int_0^{+\infty} P(f) df}} \tag{14}$$

Frequency standard deviation:

$$RVF = \sqrt{\frac{\int_0^{+\infty} (f - FC)^2 P(f) df}{\int_0^{+\infty} P(f) df}} \tag{15}$$

For physiological signals, a single time-domain or frequency-domain analysis cannot express all the valid information in the signal, and it is necessary to combine the two to extract the time-frequency domain features of physiological signals. Therefore, the wavelet transform is used to analyze the signal in time and frequency domains to extract the time-frequency domain features. The wavelet transform window function corresponds to a variable window shape, and different frequencies correspond to different resolutions, which is the main reason why the wavelet transform can analyze the non-stationary signals in both time and frequency domains. To analyze a physiological signal using discrete wavelet transform, the formula is shown below:

$$WT(a,\tau)=\int_{-\infty}^{+\infty}x(t)\cdot\psi\left(\frac{t-\tau}{a}\right)dt \tag{16}$$

where a and τ denote the scale and translation of the wavelet transform, respectively, and $\psi_{a\tau}(t)$ is the wavelet basis function.

The discrete wavelet transform can decompose the signal to different scales, and each decomposition layer contains the more hidden feature information in the physiological signal. The physiological signal wavelet is decomposed into 8 layers, the wavelet energy ratio and wavelet scale entropy of each layer are extracted, and its wavelet energy entropy and wavelet singular spectrum entropy are calculated as the time-frequency domain features of the physiological signal. In summary, a total of 39-dimensional statistical features are extracted by combining the time-domain, frequency-domain and time-frequency-domain information of the physiological signal.

3. Calculation model for assessing the psychological state of students

3.1. Construction of a multidimensional mental state calculation model

3.1.1. Support vector machines. Support vector machine (SVM) is a classification algorithm proposed based on the principle of structural risk minimization and VC dimension theory [15]. For limited sample data, SVM can find the optimal classification surface between the model complexity and the learning ability to solve the problems such as local optimal solution and overfitting of small samples in classification.

The SVM schematic is shown in Fig. 3, where the hollow circle and the solid square represent two classes, H is the classifying surface, and H_1 and H_2 are planes parallel to H and with a distance $d=2/\|w\|$ between the two planes.

Let the training dataset be: $D=\{(x_1,y_1),(x_2,y_2),\cdots,(x_M,x_M)\}$, where $x_i\in R^m, y_i=\pm1, i=1,\cdots,M$, the general expression of the class surface is shown in equation (17):

$$x^T w+b=0 \tag{17}$$

where the column vector is $x=\{x_1,x_2,\cdots,x_d\}$, the normal vector is $w=\{w_1,w_2,\cdots,w_d\}$, and the intercept is b.

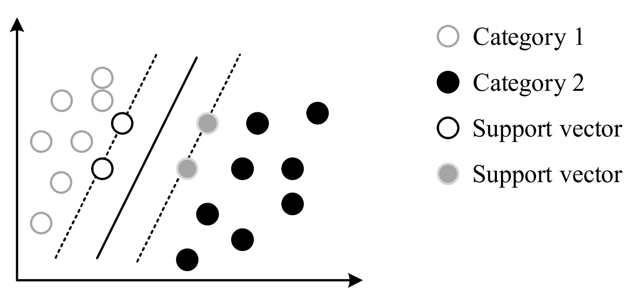

Fig. 3. SVM diagram

In order for the classification planes to classify the sample data more accurately, parallel planes H_1 and H_2 are first calculated, and then the planes centered on H_1 and H_2 are chosen as the optimal sub-planes H. Constraints:

$$x^T w+b\geq+1, y_i=+1 \tag{18}$$

$$x^T w+b\leq-1, y_i=-1 \tag{19}$$

In order to maximize the distance d between two parallel hyperplanes under the constraints of Eqs. (18) and (19), it is equivalent that the value of d^2 is maximized. i.e:

$$\max(d^2) = \min\left(\frac{1}{2}\|w\|^2\right) \tag{20}$$

When the data is linearly differentiable, the optimal linear classifier can be obtained by solving the optimal solutions of w and b satisfying the conditions through the Lagrange multiplier method [16]. Considering that many sample data are nonlinearly differentiable, it is necessary to map the data in the original space to the high dimensional space and select the hyperplane classified data with maximum spacing. The kernel function is used to map the original space data to the high-dimensional feature space, let the input space $x = \{x_1, x_2, \cdots, x_n\}$ is linearly indivisible and the high-dimensional feature space $z = \{z_1, z_2, \cdots, z_m\}$, the input space x is mapped to the high-dimensional space z by the mapping function as $\phi(x)$, and the high-dimensional space is linearly divisible, then the kernel function is as shown in Equation (21):

$$K(x,z) = \phi(x)\phi(z) \tag{21}$$

where $\phi(x)$ is the mapping function from the input space x to the high-dimensional feature space z. The parameters of the classifier can be found by finding the optimal solution of the loss function.

3.1.2. DS Theory of Evidence. The basic concepts of DS evidence theory are as follows:

Let D be the sample space and P be an arbitrary subset of D.

1) Identification frame

The identification frame is defined in the DS evidence theory used to represent all the possibilities of a given problem, usually all the discrete values of the research question.

2) The mass function (BPA)

Let the function $M: 2^{\Omega} \to [0,1]$ satisfy under the identification framework Ω:

(1) The basic probability of an unlikely event $M(\phi) = 0$ and $\phi =$ the empty set.

(2) The sum of the basic probabilities $\Sigma M(A) = 1$ and $P \subseteq \Omega$ of all the elements in 2^{Ω}, then M is said to be the probability distribution function of 2^{Ω}, while $M(P)$ is the basic confidence level of P.

3) Confidence function (Bel)

Let the confidence function $Bel(P)$ be the sum of the probabilities corresponding to all subsets in P under the identification framework Ω, i.e.:

$$Bel: 2^{\Omega} \to [0,1] \tag{22}$$

$$Bel(P) = \sum_{A \subseteq P} M(A), P \subseteq \Omega \tag{23}$$

Then the Bel function is a lower bound function, which indicates the degree of confidence in P.

According to the definition of the confidence function Bel, the expressions are shown in equations (24) and (25):

$$Bel(\phi) = M(\phi) = 0 \tag{24}$$

$$Bel(\Omega) = \sum_{A \subseteq \Omega} M(A) \tag{25}$$

4) Likelihood function (PI)

Under the identification framework Ω, for $\forall P \subseteq \Omega$:

$$PI: 2^{\Omega} \to [0,1] \tag{26}$$

$$PI(P) = 1 - Bel(\overline{P}), \forall P \subseteq \Omega \tag{27}$$

Then the PI function is an upper bound function, and P denotes the level of trust in non-false

$$PI(P) \geq Bel(P), P \subseteq \Omega \tag{28}$$

$PI(P)$ and $Bel(P)$ can divide the trust space in the sample space P into a number of subspaces with trust space $(Bel(P), PI(P))$.

In the recognition framework Ω, for $\forall P \subseteq \Omega$, the synthesis rule for the mass function $m_1, m_2, \ldots, m_n$ is:

$$(m_1 \oplus m_2 \oplus \cdots \oplus m_n)(P) = \sum_{P_1 \cap P_2 \cap \cdots \cap P_n} m_1(P_1) m_2(P_2) \cdots m_n(P_n) / K \tag{29}$$

Then the expression for K is shown in equation (30):

$$\begin{aligned} K &= \sum_{P_1 \cap P_2 \cap \cdots \cap P_n \neq \varnothing} m_1(P_1) \cdot m_2(P_2) \cdots m_n(P_n) \\ &= 1 - \sum_{P_1 \cap P_2 \cap \cdots \cap P_n \neq \varnothing} m_1(P_1) \cdot m_2(P_2) \ldots m_n(P_n) \end{aligned} \tag{30}$$

In Eq. K is called the normalization factor, which indicates the degree of conflict in the evidence.

3.2. Physiological Signal Acquisition System for Mental State Assessment

Psychological stress, also known as psychological stress, is a state of physical and mental tension manifested physiologically and psychologically when the human body is subjected to internal and external environmental stimuli. Considering that the characteristics of physiological signals cannot be concealed, the psychological stress state of the human body can be assessed objectively and effectively through the physiological signals of the human body. The psychological stress assessment method based on multimodal physiological signals in this system includes physiological data acquisition, preprocessing, feature extraction, data set division, training process, assessment process and three kinds of psychological stress assessment outputs: calm, mild stress and high pressure. The training process begins with the classification of SVM on the features extracted from a single modality, and calculates the posterior delay probability and confusion matrix based on the classification results of a single modality, as a way to construct the basic probability of DS decision layer fusion, and finally uses the DS evidence theory to make the classification judgment of the decision layer and calculate the comprehensive classification results of psychological stress under multimodal information.

3.3. Experimental design and analysis

Two sets of experiments are conducted in this paper. Experiment I compares with each single-feature SVM algorithm and multi-feature SVM-DS fusion algorithm to verify that multi-feature evaluation is more reasonable and effective than single-feature evaluation.

Experiment II compares with multi-feature SVM algorithm, artificial neural network (ANN) algorithm and SVM-DS fusion algorithm, and verifies that SVM-DS fusion algorithm is more accurate than other algorithms. Among them, the BRF radial basis kernel function is selected for SVM, and the penalty coefficient c and kernel function parameter g are optimized by the particle swarm algorithm as shown in Fig. 4.The judgment threshold ε of DS evidence theory is set to 0.47.The neural network is selected as BP neural network, the transfer function is selected as tansig, and the number of neurons in the intermediate layer is set to 14. Each set of experiments was conducted 10 times, with the training set accounting for 92% of the sample and the test set accounting for 8% of the sample.

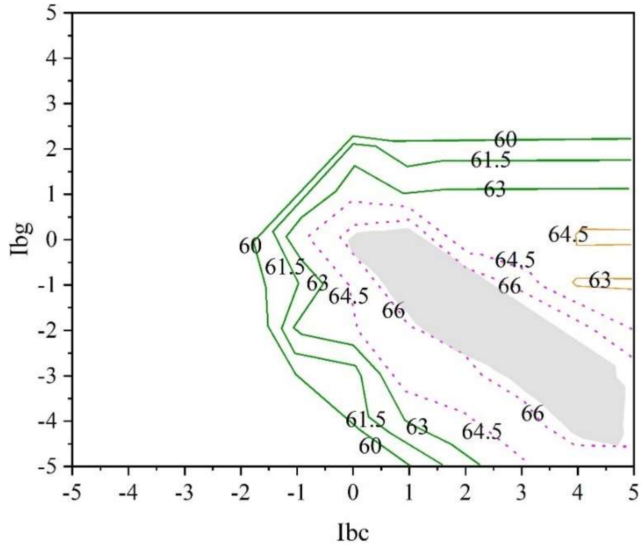

Fig. 4. Particle swarm algorithm optimizations the SVM parameter

The experimental results of the multi-feature effectiveness evaluation in Experiment 1 are shown in Table 3, and by analyzing the confidence function values, it can be seen that (1) multi-feature fusion increases the level of confidence about the correct interference effect. (2) Multi-feature fusion recognizes the correct result in the case where some single features are considered to create a conflict and thus assessed as moderate interference.

Table 3. Partial recognition framework reliability

Interference effect	Feature	Reliability function(m)			Identification result
		Light	Medium	Severity	
Light	Energy domain behavior	0.4911	0.3758	0.1267	Light
	Frequency domain behavior	0.5238	0.3577	0.1341	Light
	Time domain behavior	0.2341	0.4096	0.3609	Medium
	Anti-interference behavior	0.6901	0.2497	0.0638	Light
	Melding	0.7521	0.2488	0.0113	Light
Light	Energy domain behavior	0.5421	0.3347	0.1287	Light
	Frequency domain behavior	0.4039	0.5197	0.0796	Medium
	Time domain behavior	0.2688	0.3245	0.4113	Medium
	Anti-interference behavior	0.5276	0.3588	0.1171	Light
	Melding	0.6016	0.3927	0.0098	Light
Severity	Energy domain behavior	0.1096	0.1438	0.7491	Severity
	Frequency domain behavior	0.5027	0.0599	0.4401	Light
	Time domain behavior	0.2714	0.3275	0.4035	Medium
	Anti-interference behavior	0.1527	0.4109	0.4395	Medium
	Melding	0.0373	0.0188	0.9467	Severity
Severity	Energy domain behavior	0.5414	0.3341	0.1273	Light
	Frequency domain behavior	0.1593	0.2498	0.5937	Severity
	Time domain behavior	0.2947	0.3014	0.4075	Medium
	Anti-interference behavior	0.0625	0.2729	0.6688	Severity
	Melding	0.0547	0.2369	0.7118	Severity

Comparison of recognition accuracy of interference effects is shown in Fig. 5, which can be seen from the analysis:

The recognition accuracy of SVM algorithm with energy-domain behavior, frequency-domain behavior, time-domain behavior, and anti-jamming behavior as a single feature is low, and the recognition accuracy of SVM-DS fusion algorithm that fuses multiple features is high.

Time domain behavior has the lowest recognition accuracy due to the fact that general interference has a large coverage in the time domain range, and the tolerance of delayed interference is larger, so it is difficult to assess the interference effect through time domain behavior. The relatively high recognition rate of energy domain and frequency domain behaviors is because the interference effect is usually better when the interference power is larger, the interference frequency is aligned, and the interference style is more targeted.

The SVM-DS fusion algorithm has an average recognition accuracy of 87.8% and is more stable because the fusion approach is more adequate for extracting the elements that influence the interference effect in multiple features.

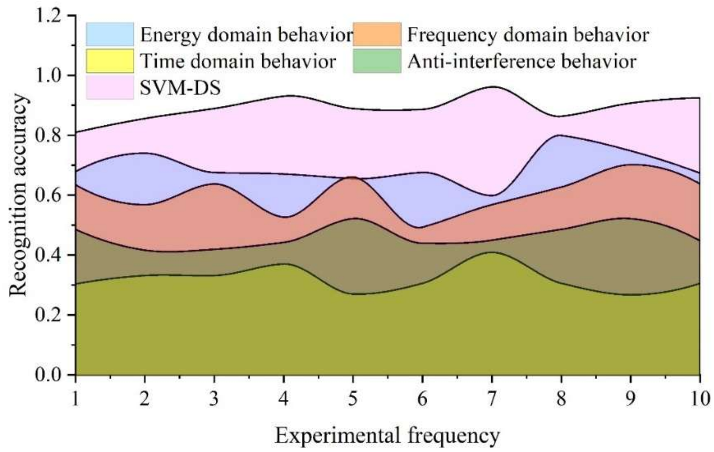

Fig. 5. The single feature algorithm is compared with the multi-feature algorithm

The recognition results of multi-feature algorithms and the comparison results of recognition rate in Experiment 2 are shown in Fig. 6 and Fig. 7 Among them, Fig. 6(a)~(c) shows the SVM-DS fusion algorithm, multi-feature SVM algorithm and ANN algorithm, respectively. It can be seen from the analysis: the SVM-DS fusion algorithm (87.8%) and multi-feature SVM algorithm (73.6%) have improved the recognition rate compared to the single-feature recognition rate, in which the ANN algorithm has a lower recognition rate due to the smaller training samples, which reflects the disadvantage of ANN in the case of small samples. While multi-feature SVM also has a high recognition rate when the number of feature dimensions increases, the algorithm is less robust, has insufficient fusion ability for incomplete and uncertain information, and is easily affected by individual singular values, which leads to poorer discriminative effect. Comparatively speaking, SVM-DS algorithm fuses the information of multiple features, while the algorithm is reasonable and simple, more stable and accurate.

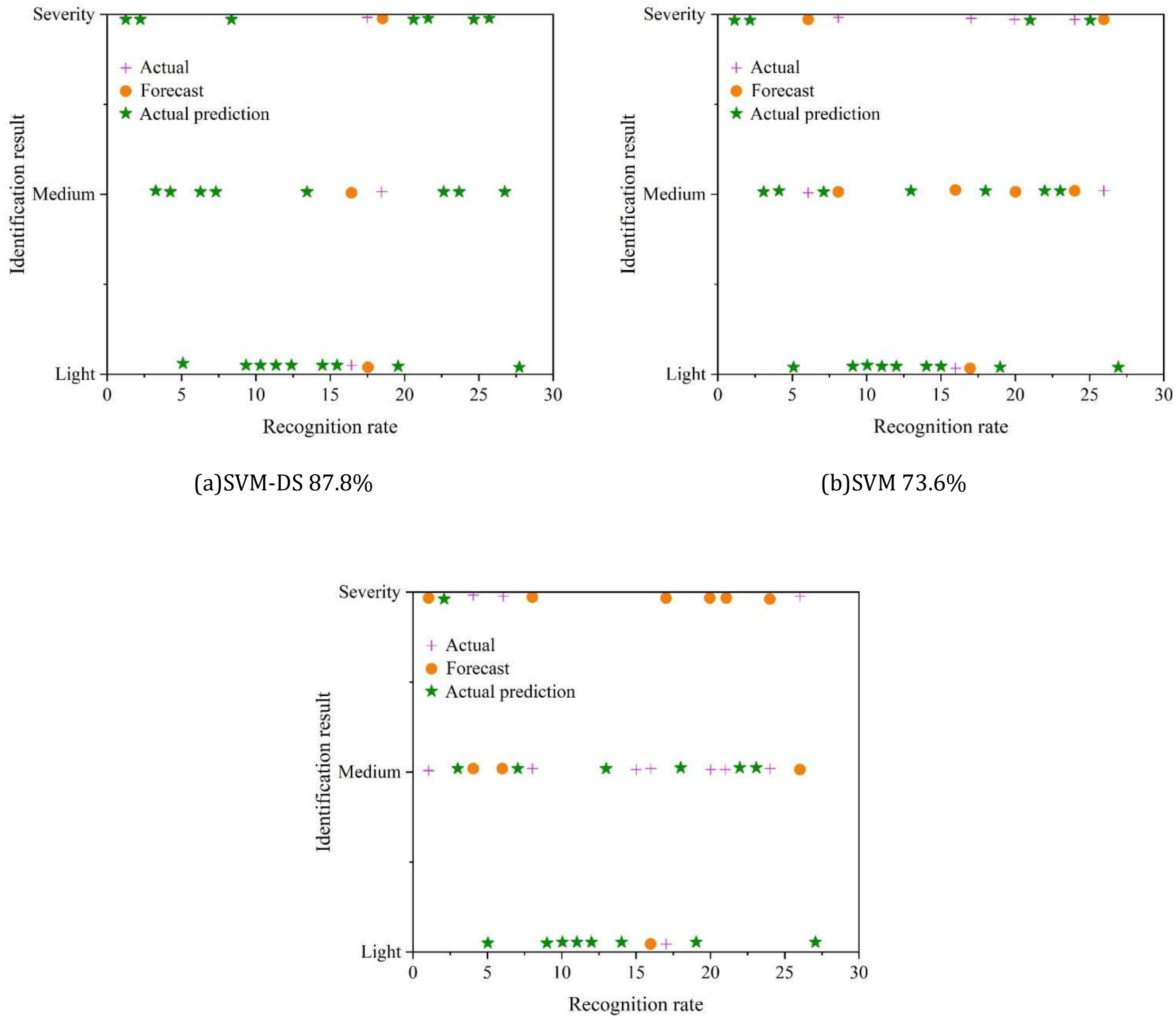

(a)SVM-DS 87.8%

(b)SVM 73.6%

(c)ANN 58.5%

Fig. 6. The results of each multi-feature algorithm in single experiment are identified

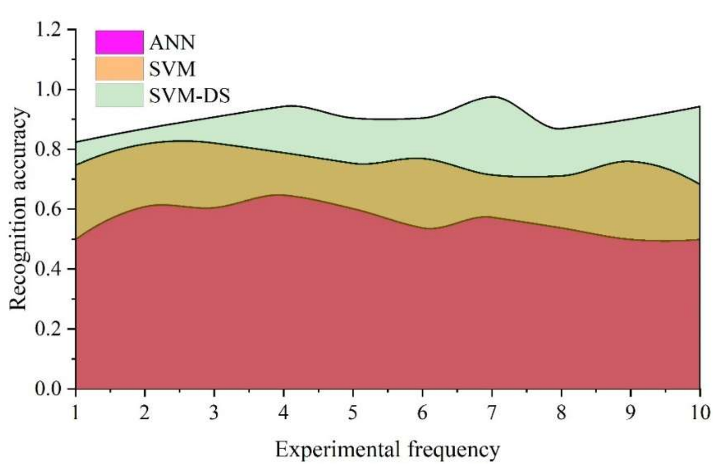

Fig. 7. The multiple feature algorithm is compared to the accuracy

4. Assessment of psychological stress states in civic education

4.1. Data Acquisition Experiments

4.1.1. Subjects and experimental environment. Subjects: A total of 115 subjects were recruited to participate in the collection of physiological data and facial video data for the psychological stress experiment. All the participants were from students (including undergraduate and master's degree students) enrolled in Civic and Political Education studies in different majors at a university, of which 69 were male and 46 were female, with ages ranging from 18 to 26, and the average age was 21. All participants in the collection participated in this experiment voluntarily.

4.1.2. Experimental Procedures. The overall process of the data collection experiment is mainly divided into the experiment preparation stage and the experiment stage. Experiment preparation stage: Subjects enter the experimental room, understand the experimental process and experimental precautions, are informed of the harmlessness of the experiment, eliminate possible psychological concerns, sign an informed consent form, allow the collection of the above data during the experiment, and register relevant information such as gender and age. Try not to move your left hand and body during the experimental test to ensure the accuracy of signal collection.

4.2. Analysis of subjective scores

Comparisons between different stimulus experiments, statistical comparisons between different subjective stress scores, subjective stress scores of different subjects overall and comparative analysis of the average time spent on different experiments.

Figure 8 shows the distribution of subjective stress scores for all the different stress test experiments, obtained from a total of 115 participants with 7 test segments each. The horizontal axis indicates the stress level, which from left to right indicates no stress, mild stress, average stress, greater stress feelings and very high stress. As can be seen from the graph, out of all the test results, 20.07% of the test sessions were considered to have no stimulus to produce any stressful feelings, about a quarter of the tests were stressful but not really strong, and less than one in ten of the test participants felt that the experiment produced a very strong feeling of stress. The overall stress arousal ratings were more at 1 and 2 so as not to produce strong stimuli for the participants and minimize the impact on their normal lives.

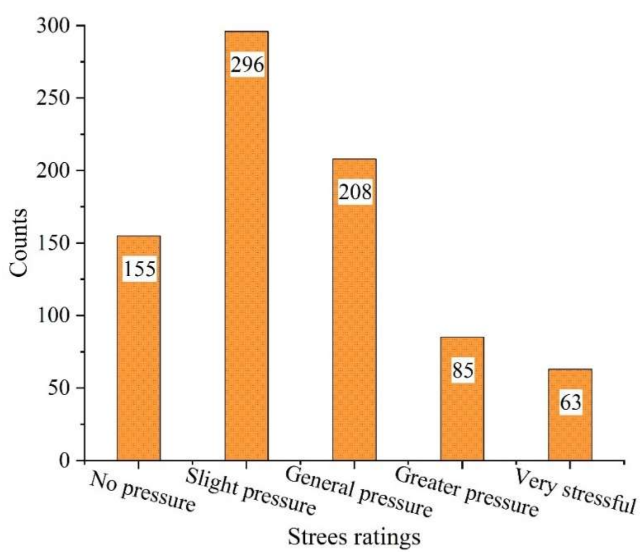

Fig. 8. Statistics of different subjective ratings

Figure 9 shows the distribution of each stressor's on the different subjective stress scores (H1: no stress, H2: mild stress, H3: average stress, H4: greater stress, H5: very high stress). From left to right, the Stroop word test (1_1), the Stroop word reversal test (1_2), the rotated letter test (2_1), the rotated letter reversal test (2_2), the digit-size test (3_1), the digit-size reversal test (3_2), and the Kraepelin test (4) (below), in order, had the following mean subjective stress scores. 1.09, 1.47, 1.25, 1.77, 1.15, 1.79, and 2.39. In the first six groups of tests, each of two adjacent groups could constitute a control, the former test being a normal test and the adjacent latter group of tests being based on the former with added cognitive processes, with the latter group as a whole having an average subjective rating value of 0.7 higher than the former group. Overall the distribution of each group of tests is not the same, for different subjects, different test stress feelings are different, almost every group of tests can stimulate the subject's sense of stress from a certain angle.

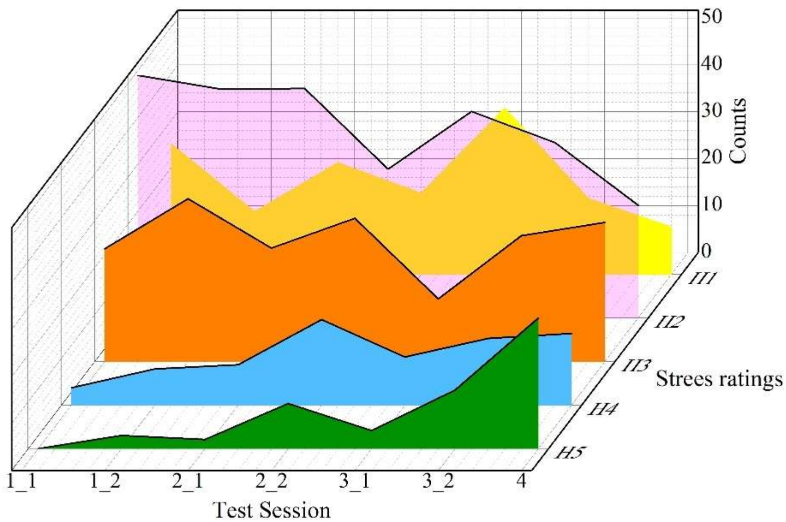

Fig. 9. Ratings of different stressors

The average time taken by each participant to complete each test question is shown in Figure 10, with error plots plotted and displayed for the time taken for the first six groups of tests only (because the first six groups were all instantaneous response judgment tests for participants, which were somewhat similar, and the final consecutive addition operation, which required a long period of time for subjects to invest their energy in participating in the computation, was not comparable to the other tests). Comparisons between each of the two groups clearly showed that the time spent on each question was overall longer with the addition of the cognitive process. The middle test of rotating letters, because it involves graphical spatial transformations and because the two alternative answers used as judgments are not in opposition to each other, makes the time required to complete these two sets of tests even greater.

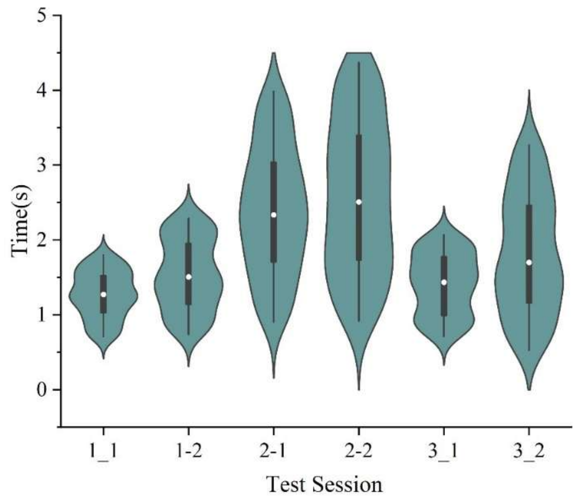

Fig. 10. Average time-consuming of the first three tests and their reversal tests

Statistical analyses were conducted for each participant's overall subjective stress scores, and the results are shown in Figure 11, which counts all seven segments of the test, with theoretical stress arousal values ranging from 0 to 28 possible. Several participants felt that none of the tests were stressful for them, and a small number had only low stress feelings overall. The majority of the feedback was within a moderate range of stress arousal, with no subjects reaching the highest stress values on all tests.

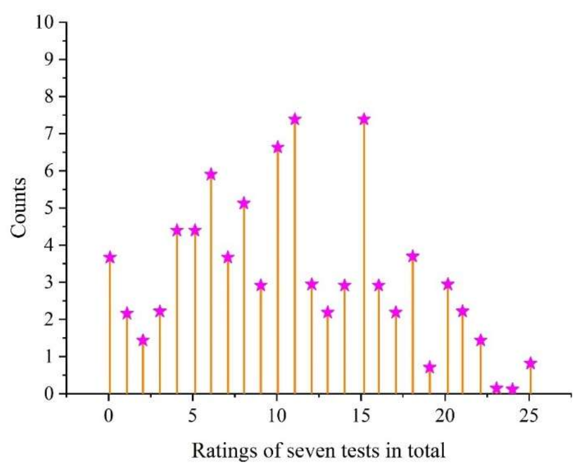

Fig. 11. The sum ratings of each subject

4.3. Correlation analysis between physiological data and subjective scores

4.3.1. Data pre-processing. The amplitude spectra of the original signals are shown in Fig. 12, (a) and (b) are the pulse and skin resistance original signals, respectively. Removing the baseline drift mainly removes the low-frequency part of it, and suppressing the high-frequency part of the signal filters out the high-frequency noise. In this paper, since the effective frequency range of both pulse and skin resistance is smaller than that of the industrial-frequency noise, high-frequency noise and industrial-frequency interference are removed directly by low-pass filtering together.

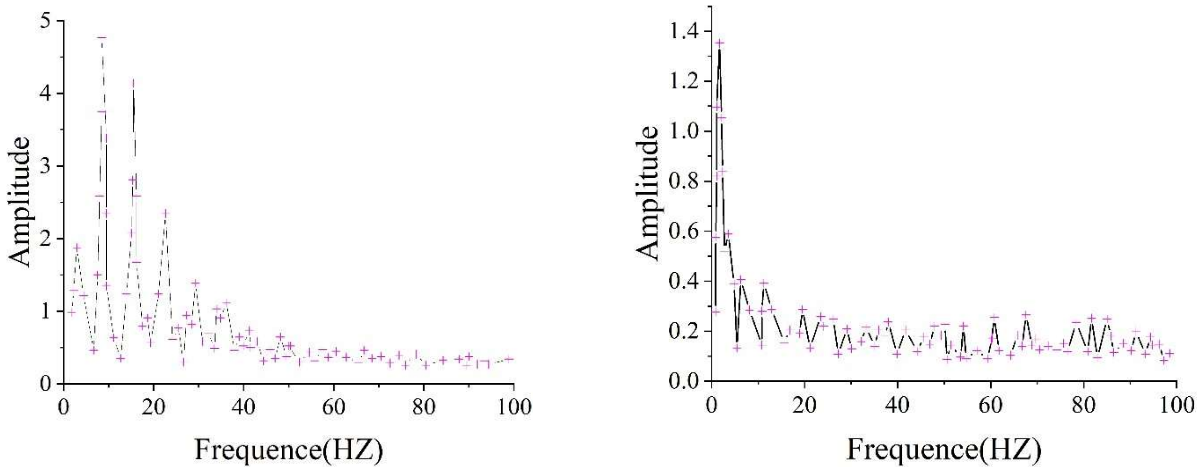

(a) Pulse primal signal amplitude (b) Skin resistance amplitude

Fig. 12. Amplitude spectrum of PPG and EDA's origin signal

A section of the pulse waveform of a subject is shown in Fig. 13, in which the original signal acquired, the signal after filtering out the high-frequency noise, and the signal after filtering out the low-frequency interference (baseline drift) are shown in order from the top to the bottom, retaining the portion of the signal with a frequency in the range of 0.23 to 21 Hz. After filtering out the high-frequency part above 21Hz, the signal becomes obviously smooth, and then filtering out the low-frequency part on the basis of this, the upward drifting part of the signal obviously falls back to basically the same height.

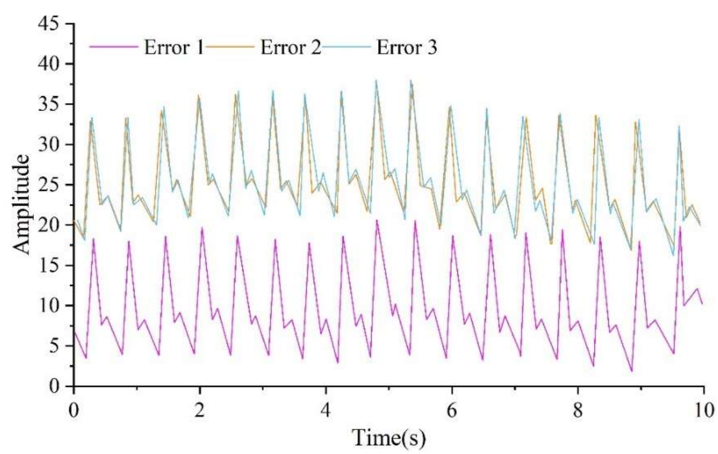

Fig. 13. Removing noise for PPG signa

Similarly for the skin resistance signal, the 0.2 to 5 Hz portion was retained and the results are shown in Figure 14. The original skin electrical signal with noise is almost impossible to see the change of skin electrical response, after filtering out the high frequency noise, the protrusion of elevated skin electrical level due to external stimulation is clearly visible, and then after filtering and removing the limit drift, the signal falls back as a whole.

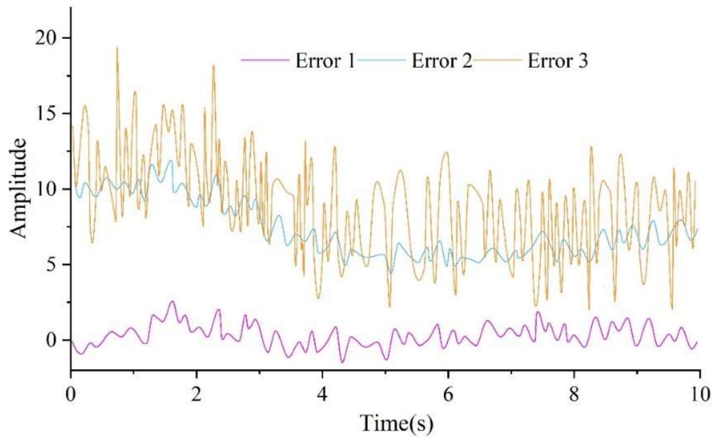

Fig. 14. Removing noise for EDA signal

4.3.2. Correlation analysis. The fast Fourier transform is used to decompose the different frequency components contained in the pulse signal, and the frequency amplitude spectral curve is plotted to analyze the frequency components of the pulse signal. The changes of the pulse signal in the time domain curve can be visualized in the shape of the corresponding spectral line. The amplitude spectra of different psychological stress test experiments and subjective scores of different stresses are shown in Figure 15, (a)~(d) are the amplitude spectra of no stress, mild stress, general stress, greater stress, and very great stress, respectively. There are obvious differences between the amplitude spectra corresponding to pulse waveforms of different psychological stress states, and there are rich spectral components, with obvious differences between the peaks corresponding to each frequency, while there are certain noise and noise components. There are obvious differences between the amplitude spectra corresponding to pulse waveforms under different psychological stress states, with rich spectral components, obvious differences in the peaks corresponding to each frequency, as well as the presence of a certain amount of noise and broad peaks.

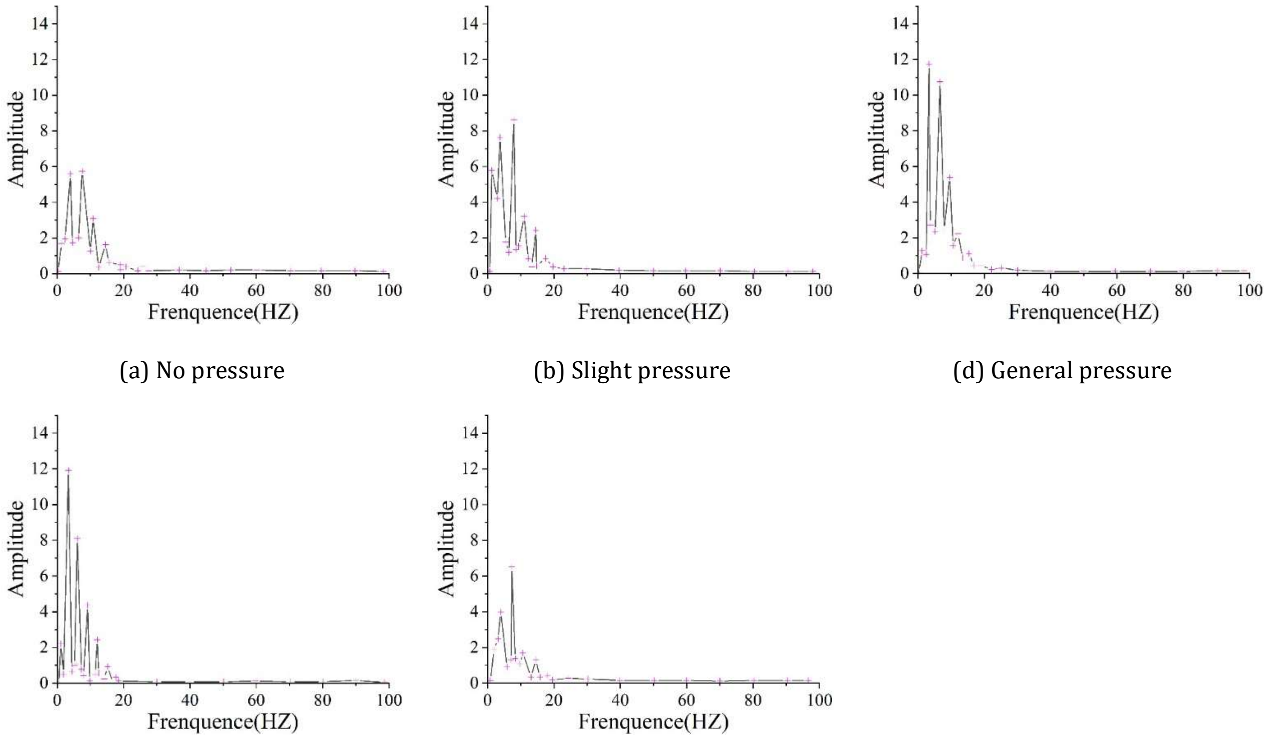

(a) No pressure (b) Slight pressure (d) General pressure

(d) Greater pressure (e) It's very stressful

Fig. 15. The PPG amplitude spectrum of one's different rating values

4.4. Feature Extraction and Feature Validity Analysis

4.4.1. Validity analysis of pulse signal characteristic parameters. The main wave crest interval of the pulse signal, which is the period of the pulse signal, was extracted as a characteristic parameter of the pulse signal, and the pulse signals of the eight testers who participated in the experiment were analyzed as shown in Table 4, and it was found that there was a significant difference between the main wave crest intervals of the pulse, which is the result of the analysis of the paired T-test of the main wave crest intervals of the pulses of the eight testers, and the significance level of the data was selected in this paired T-test as 0.05, i.e., when $P<0.05$, the data show significant difference. From the table, it can be concluded that all the testers showed significant differences ($p < 0.05$) in the pulse signal principal wave crest intervals. Therefore, the pulse signal main wave crest interval can be used as an effective characterization parameter for detecting students in different mental states.

Table 4. The main wave peak interval of the test person's pulse signal

Tester	Main wave peak interval			
	Stress-free state (mean)	Pressure is very large (mean)	t	p
NO.1	0.67	0.23	9.04	<0.05
NO.2	0.81	0.41	7.83	<0.05
NO.3	0.96	0.22	29.58	<0.05
NO.4	0.94	0.66	6.86	<0.05
NO.5	0.89	0.44	11.48	<0.05
NO.6	0.75	0.33	9.07	0.255
NO.7	0.77	0.34	8.22	<0.05
NO.8	0.96	0.18	42.28	<0.05

Figure 16 shows the peak interval of the main wave of the pulse signal of one of the eight arbitrarily selected testers. From the figure, it can be seen that the pulse signal main wave peak interval of the test persons in the fatigue state is smaller than that of their pulse signal main wave peak interval in the wakefulness state, and the difference is more obvious and easy to distinguish. Again, it shows that the interval between the peaks of the main wave of the pulse signal can be used as a valid characteristic parameter for the assessment of psychological state.

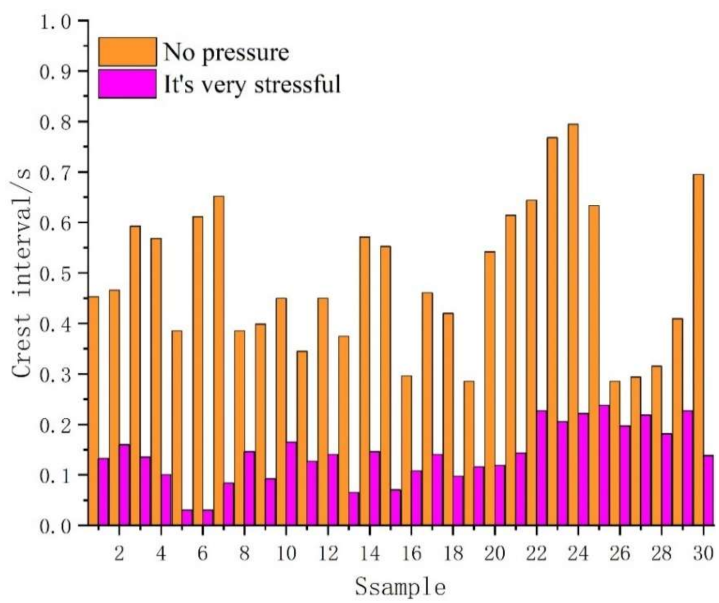

Fig. 16. One is tested for the pulse signal main wave peak interval

Further testing is shown in Figure 17. It was found that the same testers showed significant variability in their intervals at different stress states, and that the main wave crest intervals showed roughly the same trend from person to person, with all persons having lower intervals in the very stressed state than they did in the unstressed state.

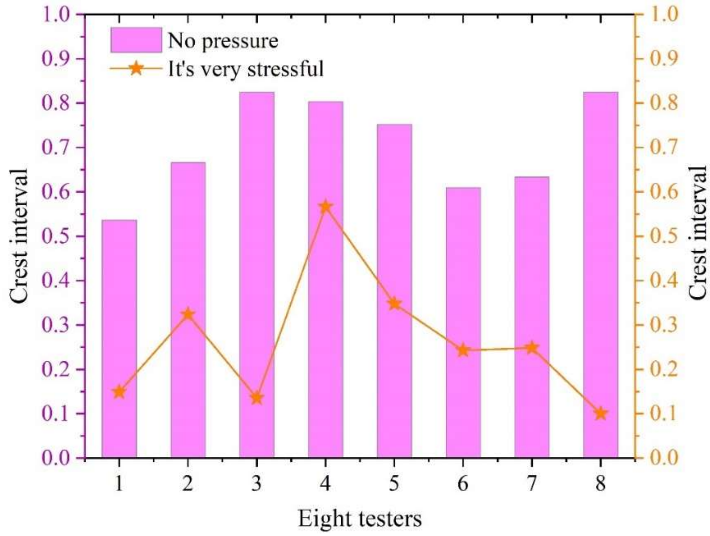

Fig. 17. Pulse signal main wave peak interval

4.4.2. Validity analysis of characteristic parameters of skin electrical signals. Eight of the participants in the experiment were selected for testing, and the results of the paired t-test analysis of the mean values of the EKG signals of the eight testers are shown in Table 5, which reveals that the mean values of the EKG signals differed from one tester to another. From the table, it can be concluded that the mean values of the skin electrical signals of all the testers showed significant differences ($p<0.05$). Therefore, the mean value of the skin electrical signals can be used as a valid characteristic parameter for detecting the psychological state of the students.

Table 5. The matching t test analysis of the mean of the skin signal in different states

Tester	The mean of the skin signal			
	Stress-free state (mean)	Pressure is very large (mean)	t	p
NO.1	0.02	0.46	8.95	<0.05
NO.2	0.02	0.94	109.63	<0.05
NO.3	0.03	0.73	-21.17	<0.05
NO.4	0.04	0.61	-18.39	<0.05
NO.5	0.57	0.15	17.06	<0.05
NO.6	0.15	0.54	-19.88	<0.05
NO.7	0.81	0.19	22.74	<0.05
NO.8	0.02	0.87	-87.75	<0.05

The mean values of the electrocorticographic signals of the eight test persons are shown in Figure 18. It was further found that although the same testers showed significant variability in the mean values of PEEK in different states, the trend of the mean values of PEEK varied from one tester to another due to individual variability, and the mean values of PEEK of the six testers, NO.1, NO.2, NO.3, NO.4, NO.6, and NO.8, were higher in the very stressful state than in the unstressed state, while the rest of testers had lower mean values in the very stressful state than in the unstressed state. The rest of the personnel had a lower mean value of PEEK in the very stressed state than in the unstressed state.

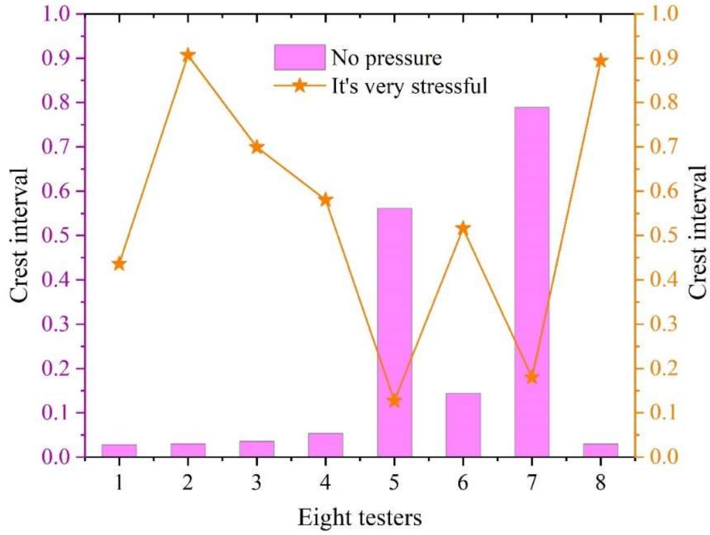

Fig. 18. The mean of the skin signal

4.5. Assessment of Students' Psychological State in Civic Education

In the first stage, SVM regression prediction is performed, which is better compared to the experimental results in the previous section.

In the second stage, the a posteriori probability is converted.The SVM-DS algorithm predicts the true value by feature regression and converts it to a posteriori probability. Figure 19 shows the distance between the classified samples and the optimal plane, and the a posteriori probability is converted to BPA to visualize the prediction of each sensor data.

In the third stage, DS rule calculation is performed.SVM-DS takes the a posteriori probability obtained from SVM as the input BPA of DS evidence theory.In this paper, the comparison of the calculation results of part of the data will be shown, in which the psychological performance has been normalized. The partial data of the model multi-feature evaluation is shown in Table 6.

As can be seen from the table, the multi-feature fusion method still performs well when some of the features conflict. Through analysis, it can be obtained that: multi-feature fusion increases the confidence in psychological performance; multi-feature fusion can still correctly realize the assessment when some single features are in conflict. The deviation of individual data from the actual psychological performance values is due to the fact that some parameters are only evaluated as BPA by normalizing the data through the experience of the experts, so the model effect does not reach the expected effect. Evaluation through the MAPE index yields an algorithmic MAPE value of 12.28%, and the assessment effect is relatively stable. The method of this paper can effectively carry out the assessment of students' psychological state in ideological and political education of college students.

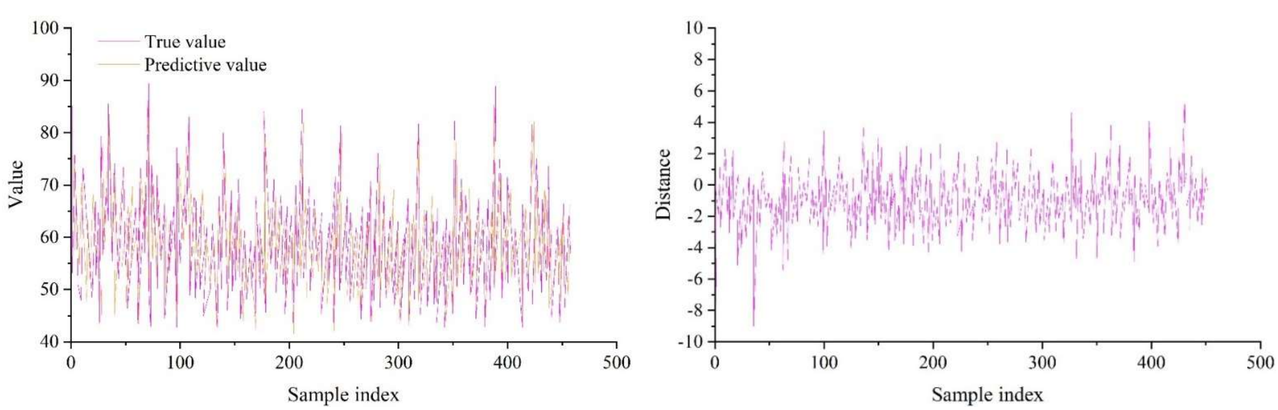

(a) SVM regression

(b) The distance from the sample to the optimal plane

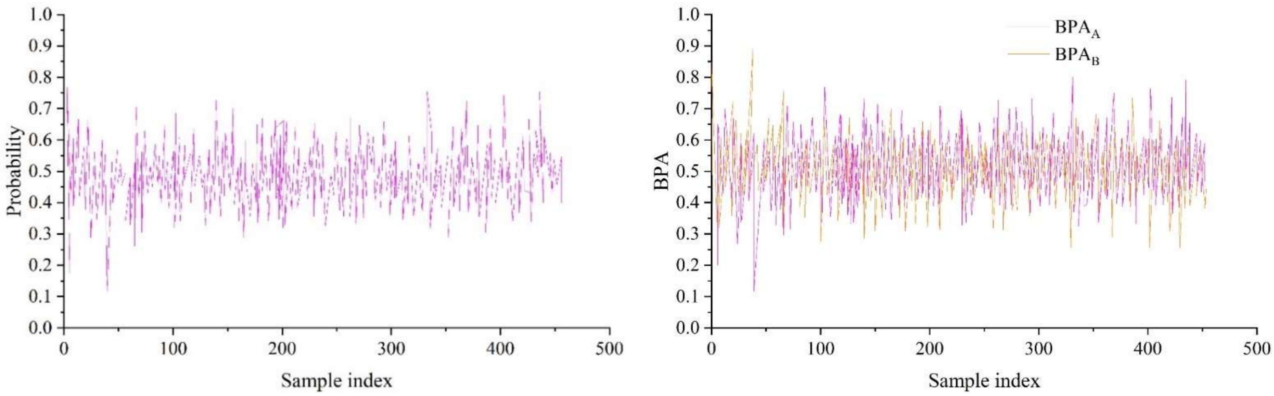

(c) Posterior probability

(d) D-evidence theory BPA

Fig. 19. SVM posterior probability conversion

Table 6. Partial sample data

Psychological performance	Ds output	BPA1 heart rate	BPA2 RPE	BPA3 thermal sensation
0.46	0.66	0.73	0.39	0.47
0.94	0.95	0.95	0.47	0.37
0.57	0.81	0.78	0.47	0.52
0.95	0.96	0.96	0.39	0.42
0.65	0.77	0.82	0.39	0.47
1	1	1	1	1
0.93	0.94	0.95	0.47	0.37
0.92	0.97	0.95	0.55	0.97
0.69	0.76	0.84	0.39	0.42
0.92	0.93	0.95	0.47	0.32
0.9	0.72	0.94	0.14	0.32
0.72	0.76	0.85	0.3	0.47

5. Conclusion

This paper proposes a physiological signal-based psychological state assessment method for students in ideological and political education of college students, which utilizes the psychological state assessment method of fusion of multi-channel physiological features to identify the students' psychological state. The signals of pulse and skin electricity are collected to extract physiological signal features. Psychological stress induction experiments were designed to establish a multimodal psychological stress detection data set for students' psychological state assessment. According to the experiments, it is shown that the recognition accuracy of SVM-DS fusion algorithm reaches 87.8%, and then the physiological signal data is filtered to remove the interference signals contained therein, and the MAPE value of the psychological state assessment using SVM-DS algorithm is 12.28%, which makes the assessment effect more stable. In summary the algorithm proposed in this paper can effectively quantify the psychological state of students and assess it in real time.

Funding

1. Research and practice project on undergraduate education reform in Henan Agricultural University: Research on the reform and practice of academy system education mode of Henan Agricultural University (2023XJGLX037).
2. Prosperous Philosophy and Social Science Application Research Project of Henan Agricultural University: Research on the construction path of counselors' studios in local agricultural and forestry colleges under the framework of "great ideological and political education" (FRZS2024B03).

References

[1] Mamurjonovich, U. T. (2024). PSYCHOLOGICAL CHARACTERISTICS OF ANXIETY IN ADOLESCENTS'RELIGIOUS-PSYCHOLOGICAL FACTORS AND UNDERSTANDING OF PROFESSIONAL IDENTITY. University Research Base, 501-506.

[2] Petzold, M. B., Bendau, A., Plag, J., Pyrkosch, L., Mascarell Maricic, L., Betzler, F., ... & Ströhle, A. (2020). Risk, resilience, psychological distress, and anxiety at the beginning of the COVID-19 pandemic in Germany. Brain and behavior, 10(9), e01745.

[3] Keles, B., McCrae, N., & Grealish, A. (2020). A systematic review: the influence of social media on depression, anxiety and psychological distress in adolescents. International journal of adolescence and youth, 25(1), 79-93.

[4] Huang, R. (2022). Research On Ideological And Political Teaching And Practice Path Of College Physical Education Curriculum From The Perspective Of Educational Psychology. Psychiatria Danubina, 34(suppl 4), 712-712.

[5] Yu, S. (2021). DYNAMIC ANALYSIS OF MENTAL STATE OF COLLEGE STUDENTS IN IDEOLOGICAL AND POLITICAL CLASS. Psychiatria Danubina, 33(suppl 6), 253-255.

[6] Shi, S. (2022). THE INFLUENCE OF COLLEGE IDEOLOGICAL AND POLITICAL EDUCATION ON COLLEGE STUDENTS'EMOTIONAL ANXIETY FROM THE PERSPECTIVE OF EDUCATIONAL PSYCHOLOGY. Psychiatria Danubina, 34(suppl 2), 201-201.

[7] Abudoukeremu, D. (2024). The Integration Path of Ideological and Political Education and Mental Health Education in Universities. The Educational Review, USA, 8(3), 469-472.

[8] Huang, H., & Liang, H. (2023). Ideological and political education combined with psychological care on patients with bipolar disorder. CNS Spectrums, 28(S2), S104-S105.

[9] Feng, X. (2021). THOUGHTS ON THE INTEGRATION OF IDEOLOGICAL AND POLITICAL EDUCATION AND MENTAL HEALTH EDUCATION IN COLLEGES AND UNIVERSITIES IN THE NEW ERA. Psychiatria Danubina, 33(suppl 8), 469-470.

[10] Feng, S. (2022). The Penetration of Personality Psychology In Ideological And Political Education In Colleges And Universities. Psychiatria Danubina, 34(suppl 1), 681-682.

[11] Li, S. (2021). The theory and practice of ideological and political education for college students from the perspective of psychology. Psychiatria Danubina, 33(suppl 6), 282-284.

[12] Wang, N. (2022). GUIDING EFFECT OF SOCIAL PSYCHOLOGY ON COLLEGE STUDENTS'IDEOLOGICAL AND POLITICAL EDUCATION. Psychiatria Danubina, 34(suppl 1), 521-522.

[13] Yang, J. (2022). RESEARCH ON THE EVALUATION SYSTEM CONSTRUCTION OF IDEOLOGICAL AND POLITICAL EDUCATION OF VOCATIONAL UNDERGRADUATE COURSES FROM THE PERSPECTIVE OF EDUCATIONAL MANAGEMENT PSYCHOLOGY. Psychiatria Danubina, 34(suppl 4), 670-670.

[14] Dževad Belkić & Karen Belkić. (2025). Optimized derivative fast Fourier transform: Splitting singlet-appearing resonances to genuine multiplets in ovarian NMR spectra from encoded time signals. Journal of Mathematical Chemistry(prepublish),1-23.

[15] David Islip,Roy H. Kwon & Seongmoon Kim. (2025). Integration of support vector machines and mean-variance optimization for capital allocation. European Journal of Operational Research(3),1045-1058.

[16] Tapas Roy & Dilip Kumar Maiti. (2025). Refined variational iteration method through optimal linear operator and Lagrange multiplier: Local/global convergence. Applied Numerical Mathematics1-28.